JOURNAL OF GEOPHYSICAL RESEARCH, VOL. 102, NO. B6, PAGES 12,187–12,203, JUNE 10, 1997

Expansion and quenching of vesicular magma fragments in Plinian eruptions

Édouard Kaminski and Claude Jaupart

Institut de Physique du Globe de Paris, France

Abstract. The conditions of pumice generation in Plinian eruptions are studied. A physical model describes the behavior of gas bubbles in a magma fragment which is carried upward in a volcanic conduit and an atmospheric eruption column. The effects of pressure release and cooling are calculated for a range of eruption conditions. The magma fragment expands in the conduit and stops expanding soon after leaving the vent, when a thin viscous rind forms against the cold mixture of magmatic gas and air. This rind prevents further volume changes. Pumice vesicularity is a function of the decompression rate in the conduit, which depends on ascent velocity and fragmentation depth. It is also sensitive to the cooling rate in the atmospheric column, which depends on vent radius and mass discharge rate. Different fragments follow different trajectories in the column and are subjected to different cooling rates. This generates a range of vesicularities which reflects the eruptive conditions. All else being equal, pumice vesicularity increases as magma viscosity decreases. These predictions are consistent with observations. Pumices provide quantitative constraints on conduit flow conditions and mass discharge rate. These concepts are applied to two Plinian eruptions. Vesicularity values for the Bishop Tuff, Long Valley caldera, require a mass discharge rate between 10^8 and 10^9 kg s^{-1}. Vesicularity variations during Plinian phase 1 of the Minoan eruption, Santorini, are explained by the conduit radius increasing from about 30 m to 120 m. Both cases require large decompression rates in the eruption conduit, suggesting that flow pressures were close to lithostatic values.

Introduction

Our understanding of explosive volcanic eruptions is extensive for atmospheric eruption columns, but remains rudimentary for the processes which occur at depth in volcanic conduits. From a given set of conditions at the vent, one can predict whether an eruption is in a Plinian or pyroclastic flow regime [*Sparks and Wilson*, 1976; *Woods*, 1988; *Valentine and Wohletz*, 1989; *Woods and Caulfield*, 1992; *Dobran*, 1992]. However, one cannot predict with confidence conditions at the vent from initial conditions in the deep magmatic system. Uncertainties arise from several sources. One is the size and shape of the volcanic conduit at depth, which determines the flow pressures. Another source of uncertainty is the process of fragmentation, such that the rising magma disintegrates into a spray. This process has been the focus of a lot of attention recently. Laboratory experiments have documented how a shock wave fragments a material [*Anilkumar et al.*, 1993; *Mader et al.*, 1994; *Sugioka and Bursik*, 1995; *Phillips et al.*, 1995; *Alibidirov and Dingwell*, 1996]. However, the scaling rules for these complex phenomena have not been established with all the necessary details, and the experiments may not be faithful analogs of the true volcanic situation. While one may anticipate key results from this line of research, it is desirable to obtain constraints on fragmentation and high-speed flows in true volcanic conduits. In this paper, we evaluate the record of eruption conditions which is provided by pumice samples.

Measurements of the volume fraction of gas bubbles (vesicularity) and textural descriptions have recently established that "dry" Plinian pumices are much more varied than previously thought [*Houghton and Wilson*, 1989; *Klug and Cashman*, 1994; *Cashman and Mangan*, 1994; *Gardner et al.*, 1996]. Significant differences in vesicularity occur between different eruptions and as a function of time during an eruption. Another important feature of Plinian deposits is that the vesicularity of pumices from a single stratigraphic level, representing an instantaneous sample of the eruption products, spans a large range of values. As emphasized by *Thomas et al.* [1994], these variations of vesicularity values imply large differences of bubble pressure which are not accounted for by existing models.

Thomas et al. [1994] have developed a quantitative model to describe the evolution of a vesicular magma

Paper number 97JB00622.
0148-0227/97/97JB-00622$09.00

fragment after fragmentation, as it is carried upward in the volcanic conduit and in the atmospheric eruption column. They did not solve for the full temperature evolution, and this provides our starting point. We add a description of processes in the atmospheric column. Another aim is to study the behavior of gas bubbles inside a magma fragment, because it may be useful for the interpretation of pumice texture. These bubbles are subjected to decompression and cooling and may end up overpressured or underpressured depending on the relative importances of these two effects.

Physical Processes Involved in Plinian Eruptions

A realistic description of a Plinian eruption must deal with the bulk flow of the mixture of gas and magma fragments and with the magma fragments themselves (Figure 1).

Volcanic Conduit

Key factors for the dynamics of conduit flow are the conduit size and how it varies with height [*Wilson et al.*, 1980; *Macedonio et al.*, 1994]. In one end-member model, the conduit walls have been eroded by the ascending mixture and have adopted an equilibrium configuration, such that flow pressures are lithostatic everywhere. In this model, the flow pressures are specified and the conduit radius is solved for. Velocities may be supersonic and reach values in the 200-500 m s^{-1} range [*Wilson et al.*, 1980]. For a crustal density of 2.7×10^3 kg m^{-3}, the decompression rate above the fragmentation level has a representative value of 10 MPa s^{-1}. In the second end-member model, the conduit size is prescribed and flow pressures are calculated. Velocities cannot exceed sonic values and are seldom greater than 150 m s^{-1} [*Wilson et al.*, 1980; *Woods*, 1995]. Above the fragmentation level, the vertical pressure gradient is typically less than 5×10^3 Pa m^{-1}, and a representative value for the decompression rate is 0.7 MPa s^{-1}, which is much smaller than in the first type of flow model.

Above the fragmentation level, the continuous gas phase expands by large amounts and would cool to very low temperatures if it was not exchanging heat with suspended magma fragments [*Giberti et al.*, 1992]. Assuming complete thermal equilibrium, *Wilson et al.* [1980] calculate a temperature decrease between 15 and 50 °C depending on the mass fraction of gas. The true value must be larger than this because many fragments are too big to equilibrate.

Eruption Column

Volcanic eruption columns have large momentum fluxes and behave as jets at small altitudes, in what has been called the "dense gas thrust" region [*Sparks*, 1986]. Cold air is entrained into the column and mixes with magmatic gas. This leads to a large cooling rate, whose magnitude depends on mass flux, gas content and vent size (Figure 2). At fixed eruption velocity, the cooling rate decreases if the conduit enlarges. For the parameters of most known Plinian eruptions, the cooling rate varies by a factor of about 2 around a mean value of 60 K s^{-1}.

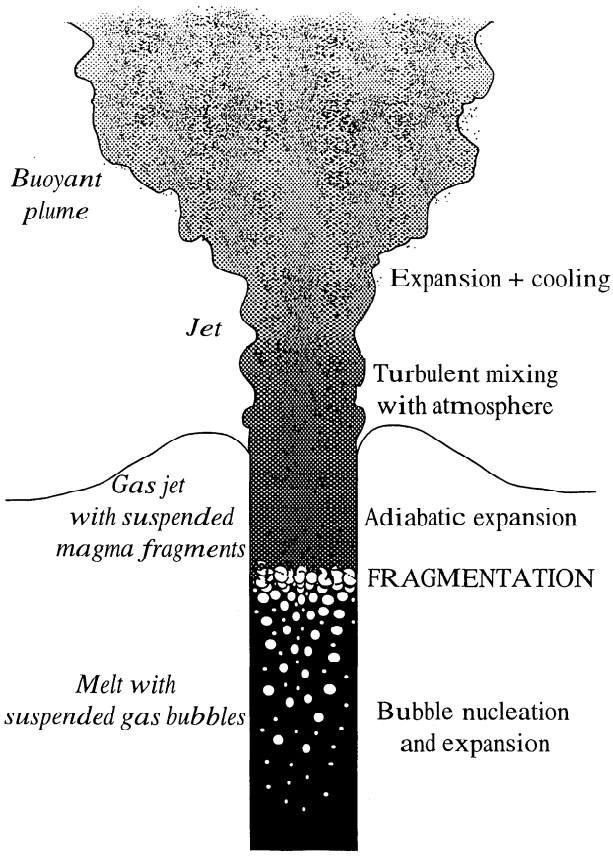

Figure 1. Illustration of the various processes involved in a Plinian eruption. Magma clasts are generated by fragmentation at some depth in the conduit. Above the fragmentation level, they undergo pressure release and small amounts of cooling due to adiabatic expansion. In the atmospheric eruption column, they are subjected to large amounts of cooling because of mixing with cold atmospheric air. The total amount of expansion depends on the relative importances of decompression and cooling.

In the atmospheric eruption column, pressure follows the atmospheric profile, which leads to a small rate of variation. In some conditions, corresponding to "fixed size" conduit models, the flow is choked. The volcanic jet issues overpressured from the vent and decompresses rapidly in the atmosphere. This late stage pressure drop is typically less than 1.5 MPa [*Dobran*, 1992] and is achieved in a few seconds [*Dobran et al.*, 1993]. This is small compared to the pressure release in the conduit, which is typically more than 10 MPa [*Thomas et al.*, 1994]. Thus, for a fragment which leaves the conduit and expands in the column, external pressure conditions cannot be distinguished from those of a constant, and small, pressure.

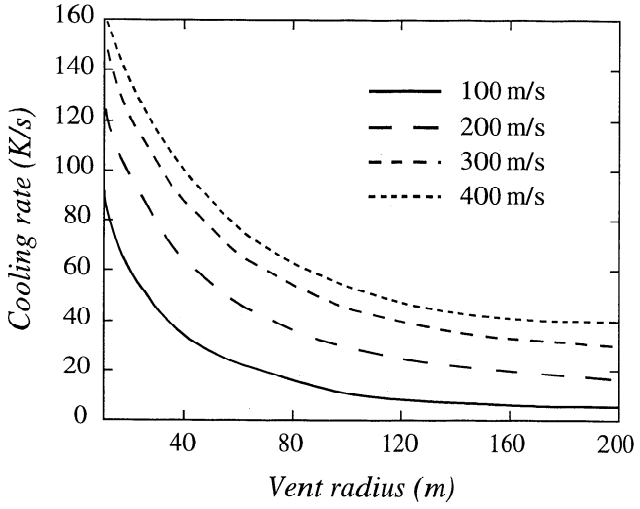

Figure 2. Average cooling rate in the atmospheric eruption column as a function of vent radius, according to the model of *Woods* [1988]. Curves are drawn for a fixed mass fraction of gas of 3 wt %. Note that the largest differences of cooling rate occur for conduit radii smaller than 100 m.

In an eruption column, all fragments do not follow the same trajectories and hence are not subjected to the same cooling rates. This provides a mechanism to generate a range of vesicularity values from homogeneous starting material. An alternative mechanism, bubble connection leading to permeability development, is discussed in Appendix A.

Vesicularity Data

When using field data, we face two different issues. One is to further our understanding of volcanic flows, and the other is to address the particulars of each eruption, for example, temporal changes of conduit size. We briefly review recent measurements on "dry" Plinian pumices and summarize the conclusions of *Gardner et al.* [1996]. Data are presented as values of the volume ratio of gas to melt, which is most sensitive to pressure. The behavior of vesicular fragments above the fragmentation level depends on the eruption dynamics as well as on the melt viscosity. At fragmentation, melt has already been degassed somewhat, and this must be taken into account when estimating viscosity. For eruptions involving different magmas with mass discharge rates varying in a restricted range, the average gas/melt volume ratio of pumices correlates with the "degassed" magma viscosity (Figure 3). The range of gas volume ratios in a deposit is a decreasing function of magma viscosity (Figure 4). Not shown here is the systematic increase of pumice vesicularity during Plinian phase 1 of the Minoan eruption, Santorini volcano, because it has already been discussed at length by *Thomas et al.* [1994]. Our basic information is therefore three fold: pumice vesicularity depends on the viscosity of magma, varies within a rather large range even in a single stratigraphic level, and may change with time during an eruption. We shall see that these characteristics provide surprisingly strong constraints.

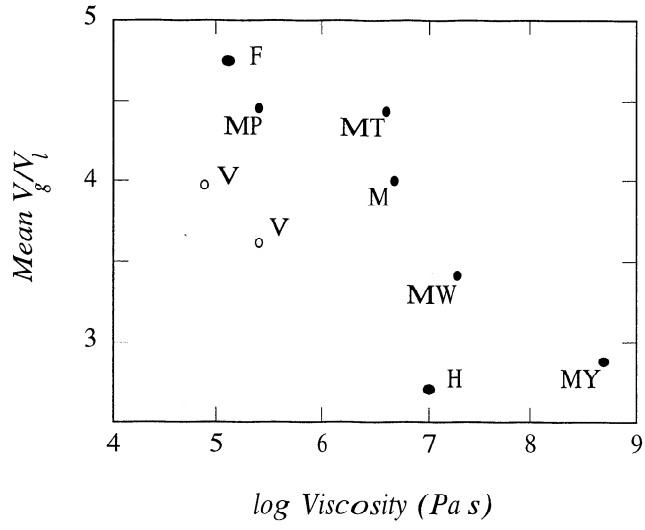

Figure 3. Mean gas volume ratio of pumices from "dry" Plinian eruptions as a function of "degassed" magma viscosity. The mass discharge rates of all these eruptions were in a restricted range of 10^7 - 2.5×10^8 kg s^{-1}. Solid circles correspond to the Hatepe (H), Fogo (F), Middle Pumice (MP), Minoan (M), Mount St. Helens T (MT), Wn (MW) and Yn (MY). Open circles (V) correspond to the two main phases of the 79 A.D. Vesuvius eruption, which went through large changes of magma composition. Data are taken from *Houghton and Wilson* [1989] and *Gardner et al.* [1996]. "Degassed" magma viscosity correspond to estimates at fragmentation and are based on the empirical scheme of *Shaw* [1972]. These estimates must be regarded as accurate to within a factor of about 5.

Physical Model

Several features of pumices may be studied, including vesicularity, vesicle shapes, and vesicle sizes. We restrict our attention to vesicularity because a large data

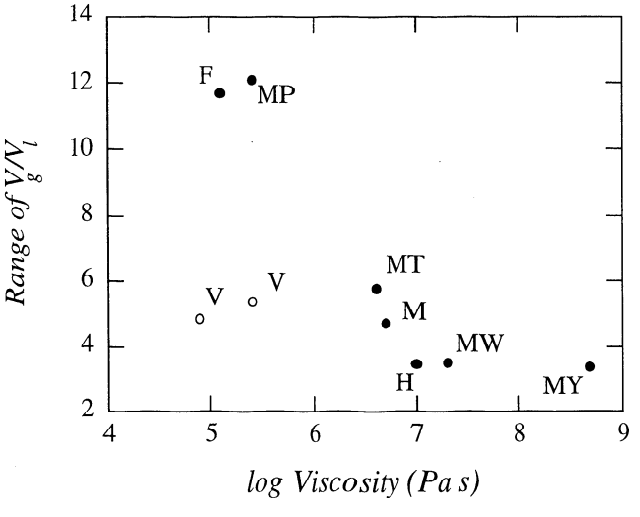

Figure 4. The total range of gas volume ratios for the same "dry" Plinian eruptions as in figure 3.

set is now available and because the quantitative prediction of vesicle shape is beyond our present modelling abilities. Our study elaborates on the physical model by *Thomas et al.* [1994]. The basic principle is to treat a vesicular magma fragment as a continuous medium, whose physical properties are allowed to vary in space and time. The model accounts for the viscous stresses generated by the expansion of gas bubbles, and its key feature is that pressures in a bubble and in the liquid around it are not equal. For simplicity, the fragment is spherical and is studied in a frame of reference which moves with it (Figure 5). In this way, we only solve for the internal evolution of the fragment and spherical symmetry is maintained. The velocity field is radial and described by $v(r,t)$. Variables are the local values of vesicularity, ϵ, pressure, p, temperature, T, and all depend on radius and time (Figure 5). Changes of external pressure and temperature are specified.

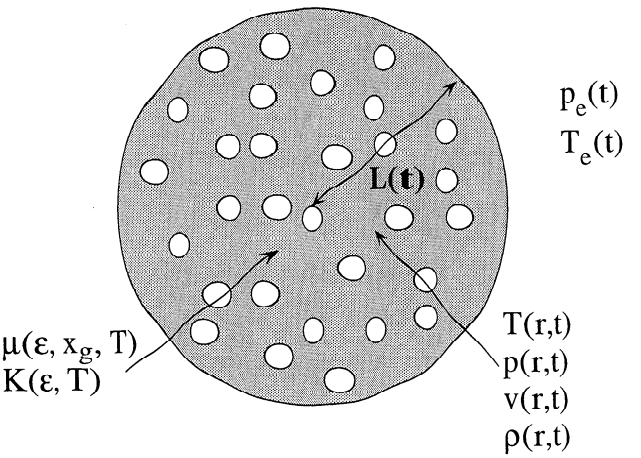

Figure 5. The various variables and physical properties used to describe the evolution of a vesicular magma fragment.

Basic Equations

We use the following relationship between stress and strain rate for the mixture of gas bubbles and viscous liquid [*Taylor*, 1954; *Prud'homme and Bird*, 1978; *Bagdassarov and Dingwell*, 1993; *Thomas et al.*, 1994]:

$$\bar{\bar{\tau}} = p\bar{\bar{\delta}} - 2\mu\bar{\bar{\epsilon}} + \left[\frac{2}{3}\mu - K\right](\nabla.v)\bar{\bar{\delta}}\,, \qquad (1)$$

where $\bar{\bar{\tau}}$ is the stress tensor, $\bar{\bar{\epsilon}}$ is the strain rate tensor, $\bar{\bar{\delta}}$ is the identity tensor, and p is the bubble pressure. The first coefficient of viscosity, μ, describes shear deformation. The second coefficient of viscosity, K, also called dilatational viscosity, introduces a difference between the local values of pressure in the gas and in the liquid. It is this pressure difference which drives the contraction or expansion of gas bubbles. For radial motion with velocity v, conservation of mass and momentum may be written as

$$\frac{\partial\rho}{\partial t} + \frac{1}{r^2}\frac{\partial}{\partial r}(\rho v r) = 0, \qquad (2)$$

$$-\frac{\partial p}{\partial r} - \frac{\partial\tau_{rr}}{\partial r} + 4\mu\frac{\partial}{\partial r}\left(\frac{v}{r}\right) = 0, \qquad (3)$$

where τ_{rr} is the radial stress component given by

$$\tau_{rr} = -2\mu\frac{\partial v}{\partial r} + \left[\frac{2}{3}\mu - K\right]\left[\frac{1}{r^2}\frac{\partial}{\partial r}(v r^2)\right]. \qquad (4)$$

To write the energy equation, we use several simplifications which are justified by *Thomas et al.* [1994]. Heat diffusion is rapid, and hence temperature is only allowed to vary on a scale much larger than the bubble size. The heat of the mixture is essentially in the liquid phase, and hence we neglect the heat content of the gas. We take into account the energy loss due to gas expansion and write

$$x_l\, C_{vl}\frac{\partial(\rho T)}{\partial t} = -\nabla.\left[x_l\, C_{vl}\,\rho\, T\, v - (p + K\,\nabla.v)\,v - k\,\nabla T\right], \qquad (5)$$

where k is the thermal conductivity of the two-phase mixture, x_l is the mass fraction of liquid, and Cv_l is the heat capacity of liquid. Thus cooling occurs because of contact against cold atmospheric air and because of the work of bubble pressure during expansion. The equation of state for the mixture is

$$\frac{1}{\rho} = \frac{x_g}{\rho_g} + \frac{1 - x_g}{\rho_l}, \qquad (6)$$

where x_g is the mass fraction of exsolved gas and ρ_g and ρ_l stand for the densities of gas and melt, respectively. The gas phase is supposed to be water and to behave ideally, such that

$$p = \frac{\mathcal{R}}{\mathcal{M}}\,\rho_g\, T, \qquad (7)$$

where $\mathcal{M}$ is the molar mass and $\mathcal{R}$ is the ideal gas constant.

Material Properties

During rapid decompression, it is likely that bubble nucleation and growth do not proceed at equilibrium [*Hurwitz and Navon*, 1994; *Proussevich et al.*, 1993]. For simplicity, such kinetic effects will be evaluated by comparing two extreme situations corresponding to different behaviors for x_g, the mass fraction of gas in the fragment. One is such that x_g remains constant, which implies that there is no bubble nucleation and that diffusion contributes little gas to the existing bubbles. This approximation is reasonable for the very short times of interest here, as discussed by *Thomas et al.* [1994]. In the other extreme, diffusion and nucleation are very efficient and keep the melt just at saturation. In this case, x_g is set equal to $x_o - x_w$, where x_o is the initial water concentration and x_w is the local time-dependent concentration. The concentration x_w is given by the empirical solubility law

$$x_w = s\sqrt{p}, \qquad (8)$$

where s is equal to 4.11×10^{-6} $Pa^{-1/2}$.

Thermal conductivity depends on temperature and gas volume fraction. At high temperature, radiation is in principle the dominant mechanism of heat transport. However, magma contains bubbles and crystals which scatter photons and hence cannot transmit thermal radiation efficiently. *Bagdassarov and Dingwell* [1994] have measured a thermal conductivity of 0.2 W m^{-2} in magmatic foams. This value is close to that for phonon conduction in silicate melts [*Snyder et al.*, 1994] and is used in most of our calculations.

The liquid viscosity, μ_l, varies with temperature according to the following law [*Richet*, 1982; *Neuville et al.*, 1993; Neuville, personnal communication, 1996]:

$$\mu_l(T) = \mu_{lo} 10^{B \frac{T_o - T}{(T - T_g)(T_o - T_g)}}, \quad (9)$$

where μ_{lo} is viscosity at the initial temperature T_o. Coefficients B and T_g are determined in the laboratory. Three different cases are considered, corresponding to phonolitic, andesitic, and rhyolitic melts (Table 1). We also consider the effect of dissolved water content on melt viscosity. Available data are few, and we take a simple equation:

$$\mu_{lo} = \mu_o \ \exp\left[-\beta\,(x_w - x_o)\right], \quad (10)$$

where μ_o is the melt viscosity at the initial water content x_o. Coefficient β is such that viscosity increases by a factor of 10 for each weight percent exsolved.

Dilatational viscosity is calculated using a two-phase model originally developed by *Prud'homme and Bird* [1978]. The resulting expression, given below, reduces to known values in the limits of small and large gas fraction [see *Thomas et al.*, 1994]:

$$K = \frac{4}{3}\mu_l \frac{1-\epsilon}{\epsilon}, \quad (11)$$

where μ_l is the viscosity of the liquid phase. The first coefficient of viscosity is more difficult to specify [see *Stein and Spera*, 1992; *Li et al.*, 1995]. If bubbles deform due to shear, it may be approximated by

$$\mu = (1-\epsilon)\ \mu_l. \quad (12)$$

Surface tension may resist bubble deformation, in which case one should write

$$\mu = \left(\frac{1}{1-\epsilon}\right)^{\frac{5}{2}} \mu_l. \quad (13)$$

There is no general expression valid in all cases. Fortunately, in the present problem, expansion induces little shear deformation, and one expects that the first coefficient of viscosity has a small impact on the model results. This was confirmed by calculations made with each viscosity expression.

The main uncertainty of the physical model is in how viscosity depends on the volume fraction of gas and on crystal content. However, the same uncertainty affects the interpretation of data. The model framework is robust and can include new experimental constraints.

Table 1. Viscosity Parameters for Three Types of Melt Composition

Melt Composition	B, $\times 10^{-3}$	T_g, K
Andesite, μ_1	7.185	508.7
Phonolite, μ_2	11.513	291.4
Rhyolite, μ_3	19.181	22.3

Method of Solution

The general problem with variable viscosity requires numerical techniques. The fragment is expanding and hence has a moving boundary whose position must be solved for. The equations are recast as a function of dimensionless variable:

$$\eta = \frac{r}{L(t)}. \quad (14)$$

Boundary conditions at $r = 0$ are derived in Appendix B. Boundary conditions at the outer edge of the fragment, i.e., at $\eta = 1$, are the values of external pressure, $p_e(t)$, and temperature, $T_e(t)$. These depend on the large-scale dynamics of the eruption. Separate pressure and temperature paths are specified for the conduit and for the atmospheric column. Equations are solved using centered finite differences for radial derivatives and a fourth-order Runge-Kutta scheme for time increments.

Viscous Quenching of Magma Fragments

Basic Framework

In this section, we focus on the atmospheric eruption column. There, as discussed above, external pressure conditions cannot be distinguished from those of a constant, and small, pressure. We start the calculation at the vent and specify the values of the various variables there. At the vent, bubbles in a fragment are overpressured with respect to surrounding magmatic gas because of earlier viscous retardation [*Thomas et al.*, 1994]. For clarity, we consider a constant cooling rate in the atmospheric eruption column and postpone the study of more realistic cooling conditions to a later section. The calculation requires five input parameters: Δp, the bubble overpressure at the vent; γ, the fixed cooling rate; μ_l, the magma viscosity; ϵ_i, the initial vesicularity of the fragment (i.e. at the vent); and L_i, the initial radius of the fragment. The effect of changing the value of ϵ_i is straightforward [*Thomas et al.*, 1994], and we shall only show results for one particular value, 60%. We shall see that the initial size of the fragment has a weak effect, and we shall emphasize the remaining three parameters, Δp, γ and μ_l.

Table 2. Standard Eruption Model Used to Study the Evolution of Magma Fragments in the Eruption Column

Parameter	Value
Melt composition	Phonolite with 4 wt % H_2O
Initial melt viscosity μ_l	$2\ 10^7$ Pa s
Initial vesicularity ϵ_i	60%
Initial overpressure Δp	20 MPa
Conductivity k	0.2 W m^{-1} K^{-1}
Cooling rate γ	100 K s^{-1}
Initial radius L_i	0.1 m

A Numerical Experiment

A fragment leaves the volcanic vent with a bubble overpressure of 20 MPa and is cooled at a constant rate of 100 K s^{-1}. Melt has an initial viscosity of $2x10^7$ Pa s (Table 2), and its viscosity varies with temperature according to the "phonolitic" function (see above).

The temperature evolution is straightforward: a cold boundary layer grows at the edge of the fragment (Figure 6). At small times, expansion is homogeneous because there is little temperature variation. Cooling induces three effects. The gas phase tends to contract. The temperature decrease induces a local increase of viscosity which slows down bubble dilatation. Thus the volume fraction of gas increases less rapidly in the rim than in the interior of the fragment (Figure 7), and a gradient of vesicularity develops. Finally, the viscous rind acts to impede the expansion of the whole fragment. After a short time, this prevents further volume change, and the fragment is "quenched" viscously before temperature reaches the glass transition. Subsequently, temperature continues to decrease (Figure 6). Vesicularity stays constant, and bubble pressures continue to decrease at constant volume (Figure 6).

It takes a few seconds to stop expansion in the atmospheric eruption column (for observations relevant to this result, see *Thomas et al.* [1994]). We found that this "viscous quench" effect is not sensitive to the rind thickness. The critical effect is that the outer edge temperature drops below a certain value, such that viscosity reaches a threshold value. One consequence is that the final vesicularity does not depend on the radius of the fragment, in agreement with the observations [*Houghton and Wilson*, 1989; *Gardner et al.*, 1996]. Another consequence is that the thermal conductivity value needs not be known with high accuracy. To verify this point, we carried out calculations with conductivity values varying between 10 and 0.1 W m^{-1} K^{-1} and found that the results differed by small amounts.

An Approximate Quenching Temperature

The calculations show that expansion stops when the liquid viscosity at the outer surface reaches a value of about $5x10^{10}$ Pa s. This threshold value is valid for the decompression rates reached in Plinian eruptions and would not be relevant for other cases. A simple expression for the quenching time is

$$t_q = \frac{\Delta T}{\gamma}, \tag{15}$$

where ΔT is the temperature difference required to bring the melt viscosity to the threshold value and γ is the cooling rate. The quenching time depends on

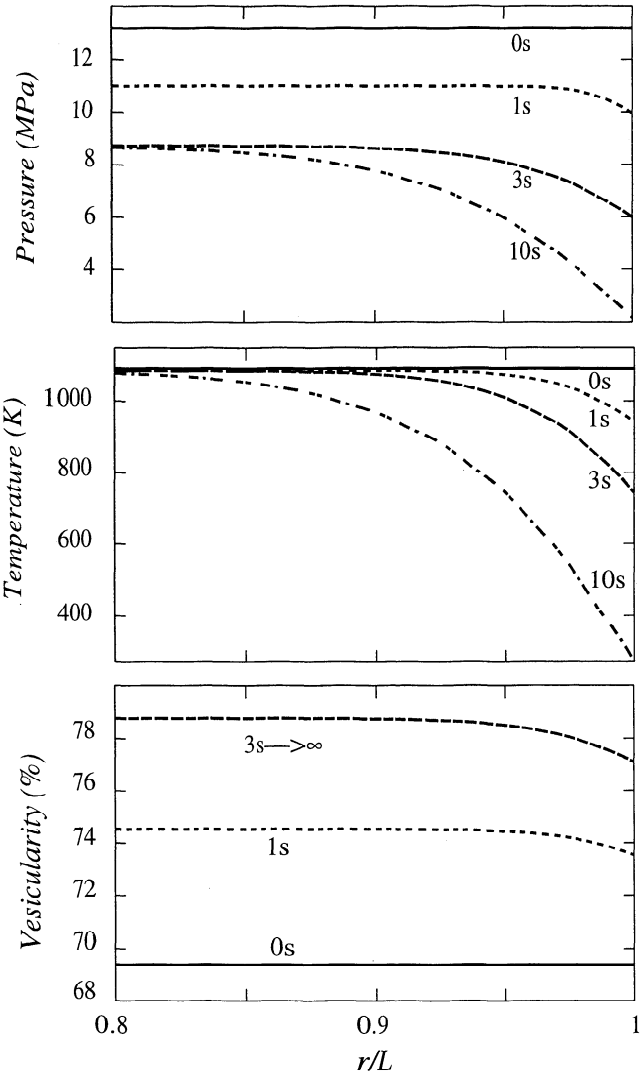

Figure 6. (top) Radial profiles of bubble pressure at different times in a magma fragment for the model parameters of Table 2. The effect of expansion dominates at small times and bubble pressures are quite uniform through the sample. After viscous quenching, the bubble pressure decreases due to cooling only and varies in a boundary layer at the edge of the fragment. (middle) Radial profiles of temperature for the same calculation. Note the progressive decrease of the exterior temperature and the growth of a cold boundary layer at the edge of the fragment. (bottom) Radial profiles of vesicularity for the same calculation. Vesicularity increases with time everywhere but not at the same rate. A gradient of vesicularity develops at the edge of the fragment.

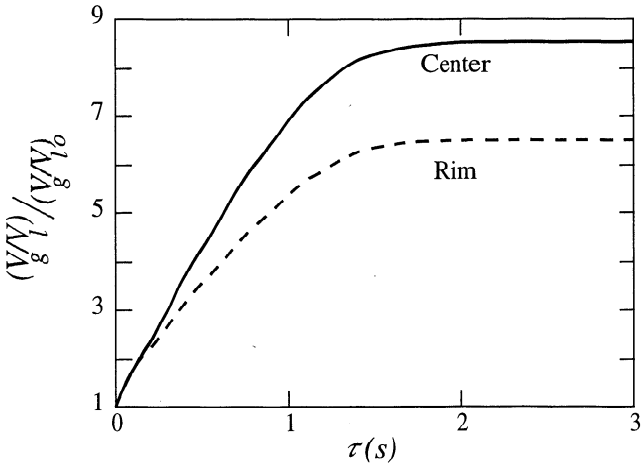

Figure 7. Evolution of gas volume ratio (normalized to the initial value) as a function of time at two locations in the fragment: the center ($r = 0$) and the rim ($r = L(t)$).

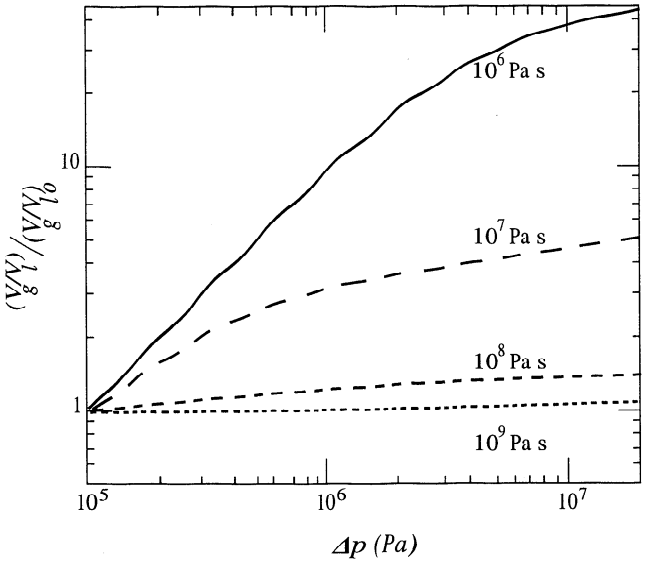

Figure 9. Final value of gas volume ratio (normalized to the initial value) as a function of the imposed pressure drop for the model parameters of Table 2. Curves are drawn for four different values of the initial melt viscosity. Note that above a certain value of pressure drop, expansion is stopped by viscous quenching before pressure equilibrium between gas bubbles and outside air is achieved.

the initial viscosity of the melt and on the extent of degassing as pressure is released. Figure 8 shows the values of ΔT for the three viscosity functions of Table 1 and for different amounts of exsolved water (0, 1, and 2 wt %). All else being equal, the larger the initial viscosity, the smaller the quenching time.

Parametric Study

The amount of expansion is obviously an increasing function of initial bubble overpressure at the vent, Δp (Figure 9). For viscosity values larger than about 10^8 Pa s, this dependence is weak because there is little expansion. For smaller values of viscosity, one may define two behaviors. For small values of Δp, expansion nearly proceeds to completion and gas volume is an almost linear function of Δp. For values of Δp larger than about 10^6 Pa, this simple relationship no longer holds. Viscous quenching occurs after some finite pressure drop, implying that the final vesicularity is weakly sensitive to Δp.

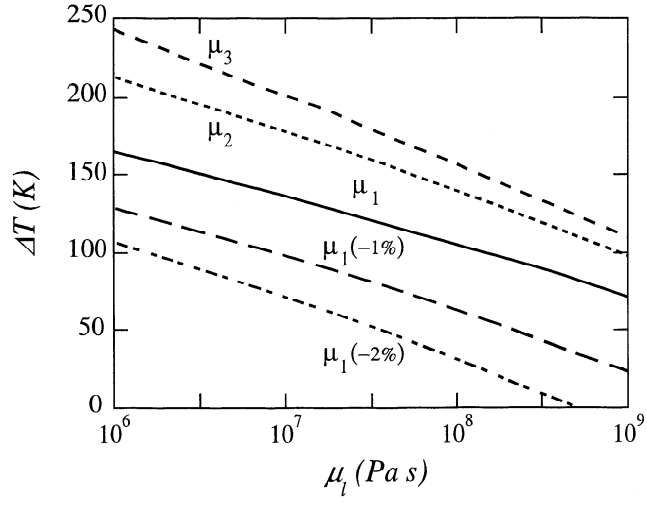

Figure 8. Temperature drop required for viscous quenching of magma fragments, as a function of initial melt viscosity. Three curves at the top show the three forms of temperature dependence defined in Table 1. The two curves at the bottom show the temperature drop required for quenching assuming that the melt degassed 1 and 2 wt % water.

The final vesicularity achieved in a fragment depends on the competing effects of pressure release and cooling. The key point is that for all Plinian eruptions, the cooling rate does not vary by more than 1 order of magnitude, whereas the rate of expansion is proportional to viscosity and hence may vary by many orders of magnitude. In the limit of small viscosity, cooling starts to operate when the fragment is already fully expanded and hence does not affect vesicularity. In the other limit of large viscosity, the fragment gets quenched before it can expand. Thus, in both limits, vesicularity depends weakly on the history of cooling (Figure 10). Large differences of vesicularity are predicted in the intermediate viscosity range of 10^6-10^9 Pa s. For known Plinian deposits, the cooling rate varies in a range of 20-120 K s^{-1} (Figure 2). It is in this range that significant differences of expansion are generated (Figure 10), and this explains why vesicularity values are so contrasted in the different deposits studied. This also emphasizes that the model parameters must be in the appropriate range for predictions to agree with the data.

Bubble Connection

Depending on the respective amounts of expansion and cooling, bubble pressures may evolve differently and

bubbles may connect by bursting or by collapsing. Because of the viscous rind, these internal rearrangements do not lead to any variation of bulk vesicularity. Critical variables are magma viscosity and decompression rate. At high viscosity or at high decompression rate, the initial overpressure is large, and cooling-induced contraction is not sufficient to decrease bubble pressures below atmospheric values. Thus, when bubbles connect, they are overpressured and lose some of their gas to the exterior. At small viscosity or at small decompression rate, magma fragments remain in pressure equilibrium until quenching. Subsequent cooling induces underpressure in the gas bubbles, which generates an inflow of outside air at the onset of connectivity.

Constraints on Eruption Dynamics

Particle Trajectories in the Atmospheric Eruption Column

The most surprising feature of Plinian deposits is perhaps that pumice vesicularity is so variable. This is true both for a whole deposit and for individual levels in a deposit. Variations over the thickness of the deposit may be explained by changes of eruption conditions, and this idea is pursued below. Variations in a single level may be due to the fact that different fragments have different trajectories in the eruption column, and hence have different histories of cooling. Models of volcanic jets are developed in Appendix C and predict significant differences between the horizontal average of temperature and the centerline temperature (Figure 11).

As shown by the previous calculations, quenching occurs at small altitudes in the eruption column. Processes in this region are therefore analogous to those of a gas-particle two-phase turbulent jet. We briefly review our current understanding of these flows [*Chung and Troutt*, 1988; *Ishii et al.*, 1989; *Eaton and Fessler*, 1994; *Prevost et al.*, 1996]. The key effect is that large particles disperse less than surrounding gas. The problem has two time constants, one for the particle response:

$$\tau_P = \frac{2\,\rho_p\,L^2}{9\,\mu_f}, \tag{16}$$

and the other for the turbulent flow field:

$$\tau_F = \frac{D_o}{U_o}, \tag{17}$$

where ρ_p and L are the particle density and radius, μ_f is the viscosity of gas, D_o is the vent radius, and U_o is the centerline velocity at the vent. The ratio of these two times, $St = \tau_P/\tau_F$ (the Stokes number), characterizes the effectiveness of large eddies for moving particles laterally. At large St, particle trajectories are weakly affected by turbulence.

St is the key dimensionless number for the dynamics of relative particle motions in the global flow parameterization. However, it does not describe the local behavior of a particle everywhere in the jet. Particle response time τ_p is a reference scale which corresponds to small relative motions between particles and gas. As the flow develops, particle velocities may deviate from those of gas by large amounts, and one may define a local response time which is smaller than τ_p by factor f [*Clift et al.*, 1978]:

$$f = 1 + 0.15\,Re_p^{2/3}. \tag{18}$$

Re_p is the Reynolds number for relative particle motion:

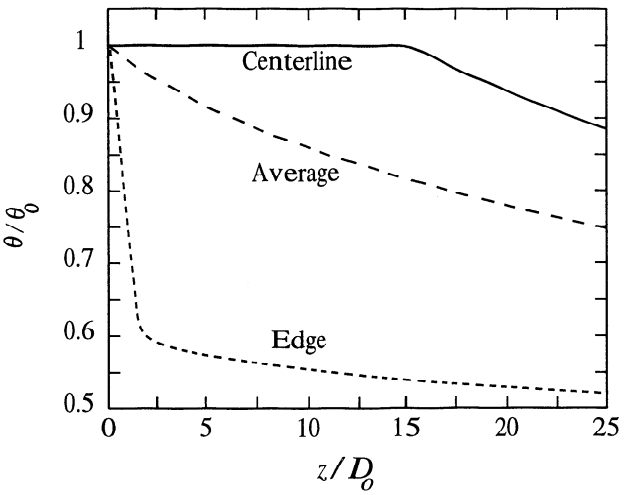

Figure 11. Temperature as a function of height above the vent in the column model of Appendix C with the parameters of Table 3 and with the entrainment law of *Woods* [1988]. Curves are shown for the average temperature in the jet and for two straight trajectories issuing from the centerline and the edge of the vent. The centerline region is affected by adiabatic expansion only between z=0 and z=15xD_o and by the entrainment of outside air at greater heights.

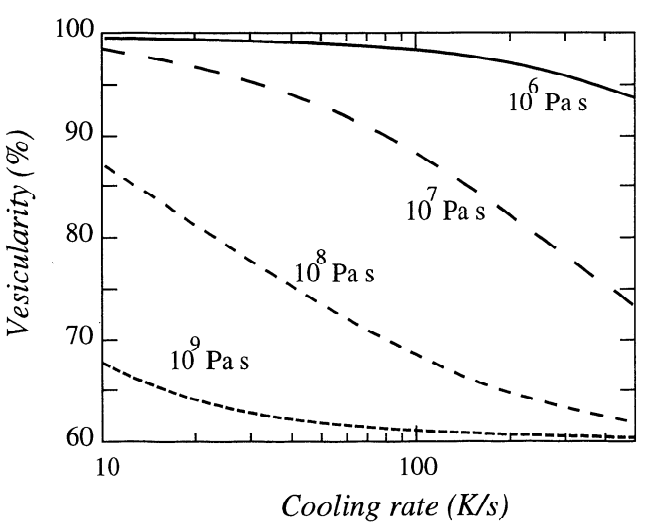

Figure 10. Final vesicularity as a function of cooling rate for four different values of the initial melt viscosity (parameters are given in Table 2).

$$Re_p = \frac{\rho_f \mid U - U_p \mid L}{\mu_f}, \qquad (19)$$

where ρ_f is the gas density, U_p is the particle velocity and U is the local gas velocity. At high particle concentration, the flow dynamics are very complicated and involve the formation of particle clouds [*Eaton and Fessler*, 1994]. In volcanic plumes, however, the volume fraction of particles is typically less than 1%, and the mixture may be considered dilute [*Hardalupas et al.*, 1989]. Most studies have dealt with monodisperse and moderately polydisperse dilute mixtures, which have the same behavior [*Prevost et al.*, 1996]. For a given St, lateral dispersion increases with increasing distance from the vent and only becomes significant at some distance noted X. A rough rule of thumb is $X/D_o \approx St$ [*Chung and Troutt*, 1988; *Ishii et al.*, 1989; *Prevost et al.*, 1996]. The extent of dispersion also depends on the initial radial position of the fragment, but this is a weaker effect.

In a Plinian column, complications may arise because of the extreme polydispersity of the volcanic mixture. Typical values for the density of vesicular magma fragments, the viscosity of hot air, the vent radius, and the centerline velocity are 700 kg m^{-3}, 10^{-5} Pa s, 100 m, and 150 m s^{-1}, respectively. Fragments with radii of 1 mm or more have Stokes numbers larger than 10. Such fragments develop significant velocity differences with respect to their surroundings, and it may be more appropriate to view them as flowing through a mixture of air and ash. An accurate assessment of such a situation is not possible with current models [*Ishii et al.*, 1989], and we develop a qualitative argument. The mixture of gas and ash is dilute, and we use the dusty gas approximation. Dusty gas is denser than pure gas but has the same dynamic viscosity [*Marble*, 1970]. If all else stays the same, this acts to increase the Reynolds number for the relative particle motion and hence to decrease the local particle response time. At large Re_p, the correction is equal to the dusty/pure gas density ratio raised to the 2/3 power (equation 18). A representative value for the mass fraction of gas in the volcanic dusty mixture is 5 wt %. In this case, the dusty gas is about 10 times denser than pure gas, and the particle response time may be decreased by a factor of about 5. As a first approximation, we may consider that a fragment behaves in fact as if its Stokes number was 5 times smaller than the "pure gas" value. For the above parameters, fragments with radii of 3 mm or more have "effective" Stokes number larger than 10. Pumice samples analyzed for vesicularity are larger than this and hence may be studied in the large St limit.

The two extreme histories of cooling correspond to fragments erupted near the axis and the edge of the vent. For the former, lateral dispersion is negligible over a height z of more than $10 \times D_o$, corresponding to a time of more than 10 s which is close to the quenching time. For the latter, lateral dispersion becomes significant at smaller heights but no less than $z \approx 2 \times D_o$. For those, quenching is almost instantaneous and in fact is not sensitive to changes of jet temperature. Some of these particles may eventually be mixed back into the core of the jet but at much greater heights, where temperatures are small. Thus they do not get reheated by large amounts. We conclude that for our purposes, it is sufficient to consider vertical particle trajectories through the jet.

Fragments going through turbulent eddies experience temperature fluctuations. The size of the largest eddies is given by the integral turbulence length-scale Λ [*Hinze*, 1975, p. 43]. Dimensionless ratio Λ/D, where D is the jet radius, increases from 0.2 at the axis to 0.4 at the edge of the jet [*Hinze*, 1975, p. 555]. Temperature fluctuates over characteristic time Λ/U, which is less than 0.3 s for the above jet parameters. This is small compared to the quenching time, and hence it is sufficient to consider a time-averaged external temperature evolution in our calculations. In exceptionally powerful eruptions, the vent must be very large, and the characteristic time for temperature fluctuations may be close to the quenching time. In this case, vagaries of the external temperature may generate some scatter in pumice vesicularity.

Figure 11 shows the variation of temperature with height along vertical trajectories in the jet. A particle which starts at the axis sees little temperature change before entrainement has reached into the core region of the jet. At the other end of the spectrum of possibilities, a particle which starts at the edge of the vent goes rapidly in contact with cold air, and hence sees a very rapid temperature drop. Starting from the same conditions as before (overpressure of 20 MPa, vesicularity of 60% at the vent), we have calculated the average and the two extreme cooling histories (Figure 12). With decreasing viscosity, the range of vesicularity values increases, which is consistent with the data of *Gardner et al.* [1996].

Three important results emerge: (1) the rate of expansion depends on melt viscosity, (2) some fragments are cooled more rapidly than others, and (3) the final vesicularity value depends on the cooling rate and hence on the radius of the eruption column.

Dynamics of Flow in the Conduit

In the conduit, we focus on the most significant effect, decompression, and assume that temperature stays constant. The calculations include a simple parameterization of conduit flow, with a fixed decompression rate, and a complete atmospheric column model (Appendix C).

As pressure is released, some water may exsolve from the melt. This acts to increase melt viscosity, and hence, as far as bulk vesicularity is concerned, there are two competing effects: the addition of gas to the bubbles and a decreased ability to expand. To evaluate

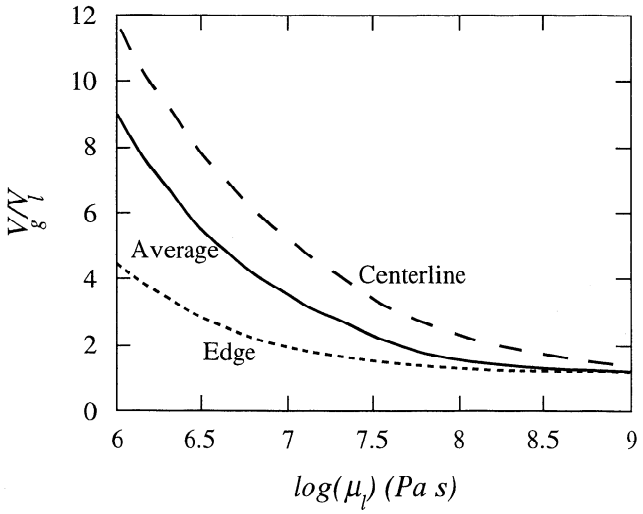

Figure 12. The gas volume ratio of pumices as a function of initial melt viscosity. The calculations are done for the model parameters of Table 3 and for the entrainment law of *Woods* [1988], as explained in Appendix C. Curves are drawn for the bulk average and for two trajectories issuing from the axis and edge of the vent. These trajectories lead to the maximum and minimum values of vesicularity and allow an evaluation of the dispersion of vesicularity values in a Plinian deposit.

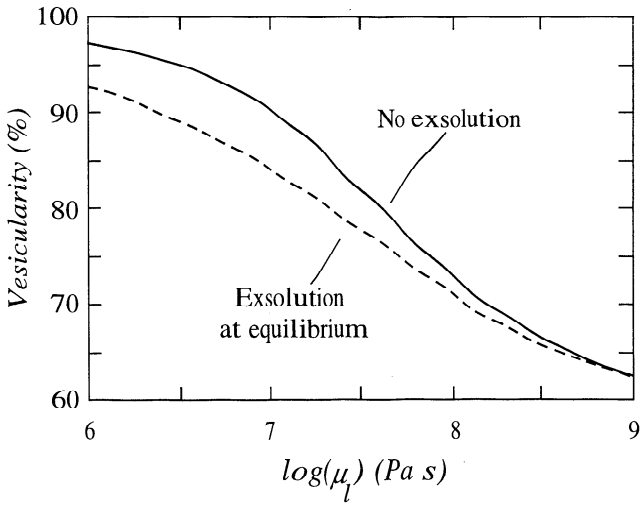

Figure 13. Vesicularity as a function of initial melt viscosity for the model parameters of Table 3. The calculations include the effects of ascent and decompression in the eruption conduit. Curves are shown for two limit cases for the melt behavior: no degassing and equilibrium degassing. The differences are small for high-viscosity melts because little pressure release is achieved in the bubbles.

the importance of this effect, we consider the two end-member cases defined above, corresponding to no degassing and to equilibrium degassing. Figure 13 shows results for the "standard" model of Table 3 and for various values of "degassed" melt viscosity. The initial water concentration was set at 4 wt %, and the amount left in solution at fragmentation is 2 wt %, corresponding to a volume fraction of exsolved gas of 60%. At high viscosity, melt degassing has a negligible effect on vesicularity because there is little expansion. At low values of viscosity, the effect is more pronounced but remains small. The reason is that degassing is a self-defeating mechanism: melt degasses because the bubble pressure decreases, but the bubble pressure can only decrease if bubbles can expand. Exsolution acts to increase melt viscosity, which reduces the amount of pressure release and hence decreases the amount of exsolution.

As explained above, decompression rates are much larger in a variable conduit size model with lithostatic flow pressures than in a constant conduit size model. To investigate the implications of this, we use the Bishop Tuff magma because of its high viscosity. Its pumices are amongst the least vesicular ones and hence are least likely to have been affected by early bubble interconnection (Appendix A). Furthermore, as just shown, a large viscosity minimizes the influence of melt degassing. Using the same fragmentation conditions as by *Thomas et al.* [1994] (Table 4), we find that vesicularity values decrease with increasing decompression rate, as expected (Figure 14). A less obvious result is the relationship between the spread of vesicularity values and decompression rate. At very small decompression rates, less than 1 MPa s^{-1}, bubble pressures remain close to the exterior pressure. When fragments are erupted into the atmosphere, they cannot expand much more, and the effects of different cooling rates are correspondingly limited. At larger values of the decompression rate, bubbles are overpressured at the vent, they have a greater potential for expansion, and hence they are sensitive to different cooling rates. Effects are nicely illustrated by the maximum vesicularity value, achieved in fragments erupted near the jet axis. For values of decompression rate between 1 and 5 MPa s^{-1}, the vesicularity of these fragments decreases with increasing decompression rate (Figure 14). In these, the bubble overpressure at the vent increases with increasing decompression rate, but cooling is rapid and stops expansion before it can effect significant changes. Above a decompression rate of 5 MPa s^{-1}, however, the bubble overpressure is so large

Table 3. Extended Eruption Model Used to Study the Evolution of Magma Fragments in the Conduit and in Atmospheric Eruption Column

Parameter	Value
Melt composition	Phonolite with 4 wt % H_2O
Initial melt viscosity μ_l	2×10^7 Pa s
Initial vesicularity ϵ_i	60%
Initial overpressure Δp	20 MPa
Conductivity k	0.2 W m^{-1} K^{-1}
Decompression rate	12 MPa s^{-1}
Vent radius	100 m
Exit velocity	300 m s^{-1}
Initial gas content in the jet	3 wt %

Table 4. Parameters Used to Model the Bishop Tuff and Minoan Eruptions

Eruption	x_o, wt %	ϵ_i, %	Δp, MPa	μ_o, Pa s	Temperature, °C
Bishop Tuff	2.2	60	27	8×10^7	750
Minoan	1.8	60	18	2×10^7	850

Physical properties are given at the fragmentation level; x_o is the dissolved water content at fragmentation; and Δp is the pressure drop between fragmentation and the atmosphere.

that expansion is faster than cooling, and the maximum vesicularity increases with increasing decompression rate.

The observed mean and range of vesicularity values are sensitive to the decompression rate, and hence provide constraints on flow conditions in the conduit. In particular, it is possible to distinguish between "constant conduit size" conditions and "variable conduit size" conditions with flow pressures close to lithostatic values.

Two Test Cases

We now pursue the implications of our model for two specific eruptions, the Bishop Tuff, Long Valley caldera, and the Minoan, Santorini. We use vesicularity data to constrain the characteristics of these eruptions and discuss independent observations. We do not attempt to explain every single pumice in a deposit. As explained in Appendix A, it is likely that some fragments become permeable before quenching, which acts to stop expansion early. This implies that the lower end of the vesicularity distribution cannot be accounted for by our model. Complications may also be due to small heterogeneities of composition and crystal content or to interaction with the cold conduit walls. Therefore we only treat the statistically significant part of the observations. We use the population defined by the mean value and a total dispersion of four standard deviations, i.e. the largest and smallest vesicularity values are equal to the mean plus and minus two standard deviations, respectively.

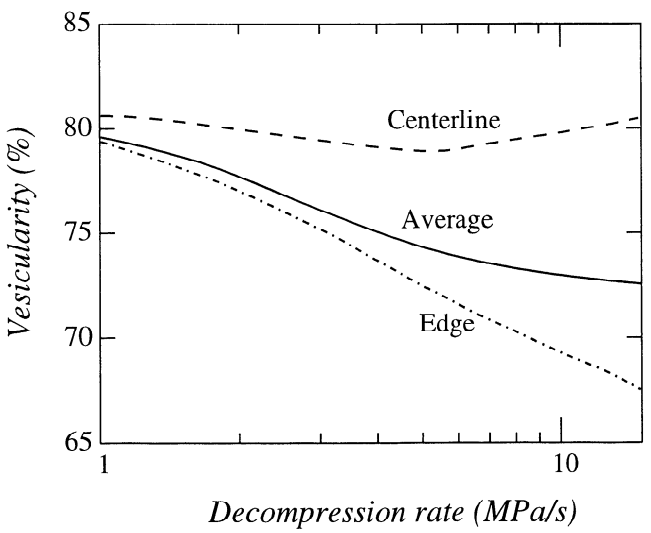

Figure 14. Final value of vesicularity for the Bishop Tuff model of Table 4, as a function of decompression rate in the conduit. The vent radius is fixed at a value of 100 m, the initial eruption velocity is 300 m s^{-1}, and the initial mass fraction of gas in the erupting mixture is 3 wt %. For this set of parameters, the mass discharge rate is 10^8 kg s^{-1}. The three curves correspond to the minimum, average and maximum vesicularity values. The total dispersion observed in the Bishop Tuff deposit is 63–79%. To achieve these values, the decompression rate must be large.

We use an initial vesicularity of 60% at fragmentation and an estimated magma viscosity. Both are subject to uncertainties. From their data, *Gardner et al.* [1996] argued that fragmentation occurs for vesicularity values in the 60-65% range and noted that this is consistent with shear-induced breakdown of a bubbly liquid. In our calculations, changing the initial value of vesicularity by a small amount, from 62% to 58%, say, simply acts to shift the final values by the same amount, and hence does not affect the range of values. Thus, we can use the dispersion of pumice vesicularities as an independent constraint. Uncertainties on magma viscosity come from several effects. One is the initial magma temperature, which is only constrained by existing methods to within a few tens of degrees. Another is the inaccuracy of empirical prediction schemes [*Baker*, 1996]. A third problem is cooling in the conduit above the fragmentation level. We thus allow for variations of viscosity from the initial estimates.

Bishop Tuff Eruption

For this eruption, we consider average, minimum, and maximum values of vesicularity of 71%, 63%, and 79%, respectively. We note that even in this high-viscosity magma, vesicularity has a large range of values. Figure 15 shows the model predictions for different values of conduit radius using the parameters of Table 4 and a fixed conduit decompression rate of 10 MPa s^{-1}. For this large viscosity value, the minimum vesicularity is not sensitive to vent size because fragments erupted at the edge of the vent get quenched almost instantaneously. If the vent radius is small, cooling is rapid

everywhere in the column, which leads to a small dispersion of vesicularity. If the vent radius is large, the core region of the eruption column stays hot for some time, and vesicularity values are dispersed.

We use two independent arguments to demonstrate that the Bishop Tuff eruption had a large discharge rate. We know that the decompression rate had to be very large, at least 10 MPa s^{-1}, say, to account for the small values of vesicularity found (Figure 14). This implies that the eruption velocity was at least 300 m s^{-1}. We also know that vesicularity values are dispersed, which implies a wide vent. The observed range of 16% requires a radius larger than 100 m (Figure 15). Combining these constraints and using a value of 10 kg m^{-3} for the mixture density at the vent, we obtain a minimum value of 10^8 kg s^{-1} for the mass discharge rate. Field determinations lead to an estimate of $8x10^8$ kg s^{-1} [*Gardner et al.*, 1991]. We now refine this comparison further.

Predicted vesicularity are slightly too high, which may be due to the magma viscosity chosen. We calculate the magma viscosity which is required to obtain a minimum vesicularity of 63%, as a function of decompression rate (Figure 16). For reasonable values between 10 and 12 MPa s^{-1}, viscosity must be in the range of $2.5 - 3.0x10^8$ Pa s. These viscosity values are higher than our initial estimate by a factor of 4, corresponding to a temperature difference of -30° C, which is within the expected error margin. Using a magma viscosity of $3x10^8$ Pa s and a mass discharge rate of 10^9 kg s^{-1}, we solve the equations for a "variable size" conduit model with lithostatic flow pressures,

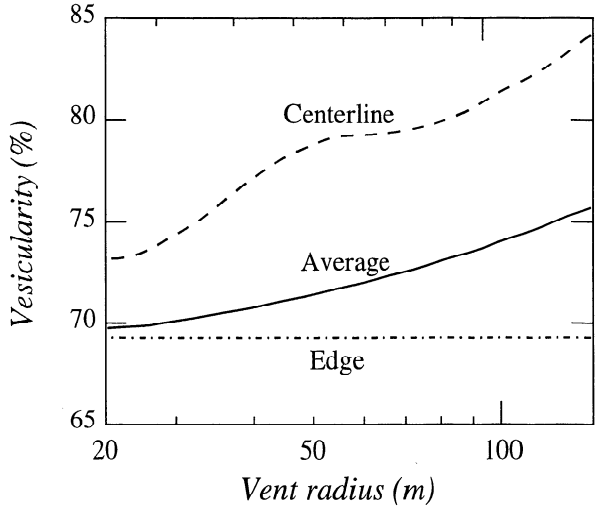

Figure 15. Final vesicularity for the Bishop Tuff model of Table 4, as a function of conduit radius. The decompression rate in the conduit is fixed at a value of 10 MPa s^{-1}. The three curves correspond to the minimum, average, and maximum values. To achieve the observed range of values, 14%, the conduit radius must be about 200 m. Smaller conduits lead to rapid cooling and a small dispersion of vesicularity values.

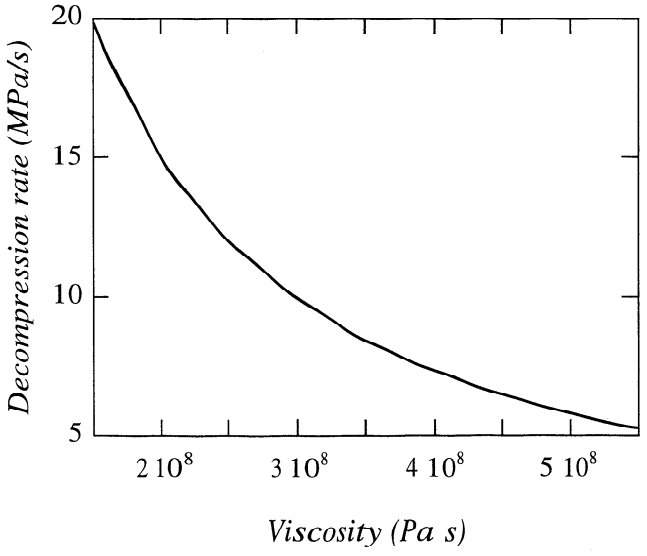

Figure 16. Decompression rate needed to achieve the minimum vesicularity of 63% in the Bishop deposit, as a function of melt viscosity. In this calculation, there is no melt degassing.

as by *Wilson et al.* [1980]. For an initial water content of 5.5 wt %, calculated decompression rates are 6 MPa s^{-1} at fragmentation and 14 MPa s^{-1} at the vent, corresponding to a mean value of 10 MPa s^{-1}. Fragmentation at 60% vesicularity releases 3.4 wt % gas. The predicted values of vent radius and exit velocity are 330 m and 440 m s^{-1}. These results provide the required inputs for the column model, and we find values of 63%, 70%, and 78% for the minimum, average, and maximum vesicularities, which are almost identical to the observed values. In conclusion, pumice vesicularities indicate a mass discharge rate of 10^9 kg s^{-1}, close to the field estimate of $8x10^8$ kg s^{-1} [*Gardner et al.*, 1991].

Minoan Eruption

Pumice vesicularity is sensitive to changes of eruption conditions, and this can be illustrated by the initial phase of the Minoan eruption (phase 1), Santorini volcano [*Bond and Sparks*, 1976; *Heiken and McCoy*, 1984]. During this phase, the eruption was in a "dry" Plinian regime [*Sparks and Wilson*, 1990], and the average vesicularity increased steadily with time [*Wilson and Houghton*, 1990]. We interpret this as due to the conduit enlarging by erosion. For our model, we use the parameters of Table 4. We find that the conduit radius increased from an initial value of about 30 m to slightly more than 100 m (Figure 17). This is consistent with the observations. The deposit is reversely graded, which shows indeed that the eruption intensity increased with time [*Heiken and McCoy*, 1984; *Sparks and Wilson*, 1990]. Also, the lithic contents of erupted material increased with time, which indicates that the conduit was being eroded [*Bond and Sparks*, 1976; *Heiken and McCoy*, 1984]. The top of the Plinian deposit records

a change of eruption conditions to a phreatomagmatic regime with abundant interaction with seawater, and it is tempting to link this with vent widening.

Discussion

Our physical model is able to explain several features of Plinian pumices: (1) the systematic decrease of vesicularity as the melt viscosity increases, (2) the dispersion of vesicularity values, (3) the systematic decrease of the dispersion of vesicularity values as the melt viscosity increases, and (4) progressive changes of vesicularity with time during an eruption. Quantitative agreement with data from the Bishop Tuff and Minoan eruptions require large values of decompression rate in the conduit and viscosity values which are slightly larger than predicted from the known magma composition and initial water content. Both points deserve comments.

The erupting mixture cools in the conduit because of expansion but also because of lithics incorporated in the flow. The consequence is that the melt viscosity must be calculated at a temperature lower than the initial magmatic temperature. A complete model should include these effects and, to be precise, should take into account the size distribution of fragments. This will be investigated in the future.

Large decompression rates are achieved in a conduit with depth-dependent size, with flow pressures close to lithostatic values. In such a case, predicted exit velocities are between 200 and 500 m s^{-1}, significantly greater than sonic values (90-200 m s^{-1}) [*Wilson et al.*, 1980]. These large velocity values are confirmed by the ballistics of large blocks found near the vents of many Plinian eruptions [*Wilson*, 1976]. These conditions are probably due to conduit erosion for which there is independent evidence in the form of lithic fragments and of temporal increases of discharge rate.

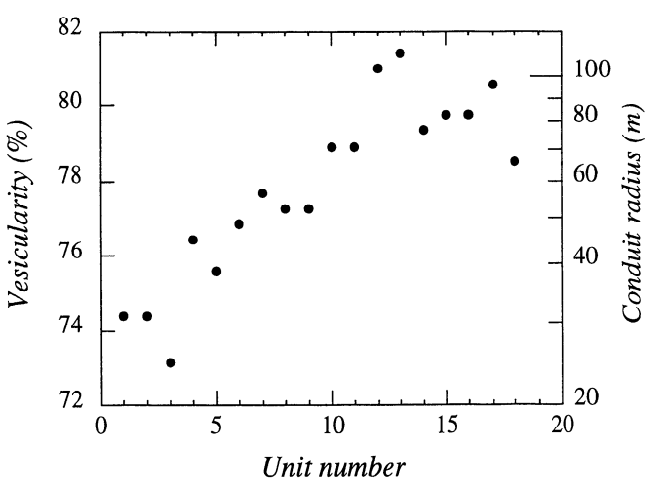

Figure 17. Average vesicularity as a function of stratigraphic height in the Minoan Plinian deposit for the model parameters of Table 4. The conduit radius which is required to produce the observed vesicularity is indicated on the right-hand axis. This example suggests that the conduit widened.

One can get three quantitative constraints on the dynamics of "dry" Plinian eruption from their deposits: the dispersal characteristics and the mean and range of pumice vesicularity values. One may also determine magma composition and initial water concentration. The dispersal characteristics allow an estimate of the mass discharge rate, which may be achieved in different ways. For a "constant conduit size" model, the exit velocity is smaller, and the vent radius is correspondingly larger than for a "variable conduit size" model. Vesicularity data allow us to distinguish between these two possibilities and hence provide constraints on the conduit size.

Conclusion

The distribution of pumice vesicularities provides constraints on flow conditions in both the conduit and the atmospheric column. Eruption column models can be checked against several types of data, but very few constraints are otherwise available for conduit flow. Vesicular magma fragments can be regarded as Lagrangian tracers which record temporal changes of pressure and temperature in the erupting mixture. Thus constraints on these changes may be derived independently of any specific flow model. It is encouraging that our calculations compare with observations only when the rates of decompression and cooling are set to realistic values. The physical framework may be refined to include more effects, such as, for example, diffusion of volatile species.

Appendix A: Connection of Gas Bubbles in an Expanding Fragment

Vesicularity values in Plinian pumices are dispersed. The explanation pursued in this paper is that different fragments have different histories of cooling in the eruption column. An alternative explanation is that fragments become permeable before quenching. In this case, a magma fragment cannot sustain large pressure differences between its interior and the exterior. In a large population, it is unlikely that all fragments are affected simultaneously. In this model, therefore, different fragments are subjected to the same pressure and temperature evolution, but become permeable at different times, after expanding by different amounts. Two arguments suggest that this cannot account for all the data.

Discriminating between the two explanations hinges on the process responsible for bubble connection. In a liquid fragment, neighboring bubbles may connect only if the film which separates them gets thinned. This may be achieved by two mechanisms. One is shear [*Li et al.*, 1995], which is not expected to be important for individual magma fragments suspended in a gas jet. The other mechanism is bubble expansion, which is relevant. The critical thickness for liquid film rupture is slightly less than 1 μm [*Vrij*, 1966; *Princen*, 1979; *Erneux and*

Davis, 1993; *Cashman and Mangan*, 1994]. For typical bubble sizes, this requires vesicularity values in excess of 95%. Such high values of vesicularity cannot be achieved in high viscosity fragments.

The second argument relies on the systematics of pumice vesicularity in Plinian deposits [*Gardner et al.*, 1996]. At viscosities larger than about 10^5 Pa s, the maximum pumice vesicularity increases as magma viscosity decreases, which is clearly consistent with expansion. These pumices are permeable when found on the ground, but bubble connection may be achieved late, because of thermal stresses during late stage cooling or following impact on the ground and burial in a deposit. For magma viscosities around 10^5 Pa s, pumices are highly inflated: vesicularity values are larger than 80% on average, and commonly exceed 90%. Below this threshold viscosity value of about 10^5 Pa s, the relationship between vesicularity and viscosity breaks down. In these low-viscosity cases, expansion is able to proceed to the very large values of vesicularity needed for bubble connection. This occurs early, when flow temperatures are still high. With most of its bubbles connected, a magma fragment is an open network of melt and tends to collapse under the action of surface tension [*Gardner et al.*, 1996]. This generates small vesicularity values which are indeed observed.

A final observation is that, in the Minoan Plinian eruption, vesicularity values increased systematically as the eruption was proceeding [*Wilson and Houghton*, 1990; *Thomas et al.*, 1994]. This is difficult to explain by early bubble connection.

Appendix B: Boundary Conditions at $r = 0$

The cooling rate remains finite at the center, and hence all terms in the heat equation remain finite. We recall that

$$\nabla^2 T = \frac{\partial^2 T}{\partial r^2} + \frac{2}{r}\frac{\partial T}{\partial r}. \tag{B1}$$

This remains finite as r goes to zero if and only if the temperature gradient is zero at $r = 0$:

$$\frac{\partial T}{\partial r}(0,t) = 0. \tag{B2}$$

Because of this, conditions in the vicinity of the origin are those of homogeneous expansion, which has been studied by *Thomas et al.* [1994], and we may deduce that

$$\frac{\partial \tau_{rr}}{\partial r}(0,t) = 0, \tag{B3}$$

$$\frac{\partial \rho}{\partial r}(0,t) = 0, \tag{B4}$$

$$\frac{\partial p}{\partial r}(0,t) = 0. \tag{B5}$$

Using the continuity equation, we obtain

$$\frac{\partial \rho}{\partial t}(0,t) = \left(-\frac{\rho \nabla.v}{L}\right)(0,t). \tag{B6}$$

The divergence term is written using the following identity:

$$\lim_{r\to 0}\frac{v}{r} = \frac{\partial v}{\partial r}(0,t). \tag{B7}$$

Finally, we use the energy equation to obtain

$$\frac{\partial \rho T}{\partial t}(0,t) = \left(-\frac{\rho T \nabla.v}{L} - \frac{(pL + K\nabla.v)\nabla.v}{L^2 x_l C v_l}\right)(0,t). \tag{B8}$$

Appendix C: Dense Gas Thrust Region of Eruption Columns

In the volcanic conduit, flow is in fully-developed turbulence. Thus, at the vent, the radial profiles of vertical velocity and temperature have a top-hat shape. As entrainment develops, these profiles gradually change to a bell shape (Figure 18). For this study, it is essential to describe these changes in order to calculate cooling rates for different particle trajectories. The radial profiles are defined by the maximum values of velocity and temperature, U_M and θ_M, at the center of the jet ($r = 0$), and a dimensionless shape function $f(r)$. This function is such that $f(0) = 1$ and tends to zero as r goes to infinity. The mass flux is written as

$$\beta U \pi D^2 = \int_0^\infty \beta U_M f(r) 2\pi r dr, \tag{C1}$$

where β is the jet density, U is the mean velocity and D is the effective jet radius. The flux of vertical momentum is

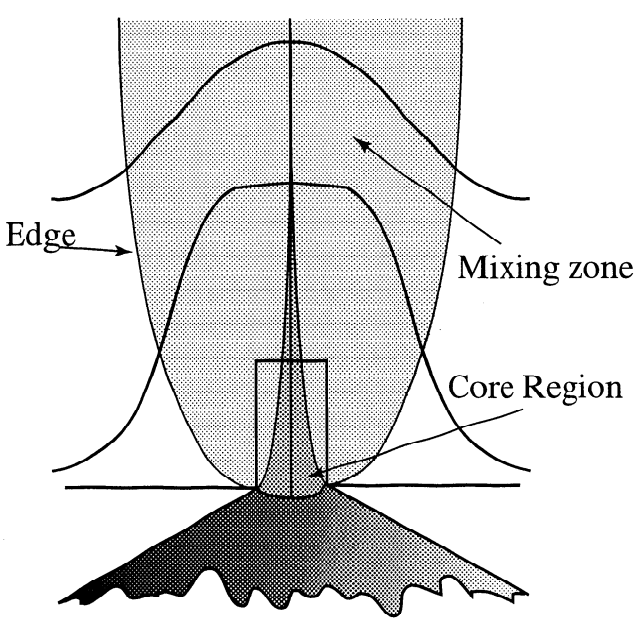

Figure 18. Evolution of velocity profile in the gas thrust region of an atmospheric eruption column. The profile becomes self similar when the mixing zone extends to the centerline.

$$\beta U^2 \pi D^2 = \int_0^\infty \beta U_M^2 f^2(r) 2\pi r dr. \quad \text{(C2)}$$

The buoyancy flux is

$$\beta C_p U \theta \pi D^2 = \int_0^\infty \beta C_p U_M \theta_M f^2(r) 2\pi r dr, \quad \text{(C3)}$$

where θ is the horizontal average of temperature. The turbulent jet entrains surrounding air with density α at rate U_e. The conservation equations are

$$\frac{d}{dz}(\beta U D^2) = 2\alpha U_e D, \quad \text{(C4)}$$

$$\frac{d}{dz}(\beta U^2 D^2) = g(\alpha - \beta) D^2, \quad \text{(C5)}$$

$$\frac{d}{dz}(\beta C_p \theta U D^2) = -\alpha U D^2 g + \left(C_a T + \frac{U^2}{2}\right) \frac{d}{dz}(\beta U D^2). \quad \text{(C6)}$$

The rate of entrainment can be written as follows [*Woods*, 1988]:

$$U_e = \lambda^* \left(\frac{U_M}{U}\right)^2 U \left(\frac{\beta}{\alpha}\right)^{0.5}, \quad \text{(C7)}$$

where λ^* is a constant which is usually taken to be 0.125. One simplification is to assume that $U_M \approx U$ [*Woods*, 1988]. This entrainment model relies on a small number of experimental studies and may be somewhat in error for particle-laden jets.

Function $f(r)$ is allowed to change with height. We use the following form:

$$f(r, z) = \exp\left(\left[-2\left(\frac{r}{\delta}\right)^n\right]\right), \quad \text{(C8)}$$

where width δ and exponent n are functions of z. At the vent, the top-hat profile is described by a large value of n. For a particle-laden jet in the self-similar fully developed region, n takes a value of about 4 [*Chung and Troutt*, 1988]. At greater heights in the atmosphere, the concentration of particles is small and the eruption column may develop into a buoyant thermal plume, for which $n = 2$ [*Turner*, 1973]. A variable exponent introduces an additional unknown, and a fourth equation is needed. At small heights above the vent, entrainment only affects the outer regions of the jet and does not reach into the core region. The centerline temperature therefore evolves by adiabatic decompression only. This is written as follows:

$$\frac{d\theta_M}{dz} = -\frac{\alpha}{\beta}\frac{g}{C_p}. \quad \text{(C9)}$$

We may now calculate all variables as a function of z. The exponent n reaches the value of 4 at $z = H$, where the dense jet is everywhere affected by entrainment. The value of H is not assumed and is calculated and depends on the vent radius. Between $z = 0$ and $z = H$, the core region of the jet expands laterally, as shown by the change of horizontal structure. For typical conditions, we find that H is smaller than the critical height at which the column may collapse, as well as smaller than the height at which the column may become buoyant. Vesicular magma fragments stop expanding before leaving the dense gas thrust region, and hence we do not follow the column into the buoyant plume regime. The model is simplified in the sense that the core and

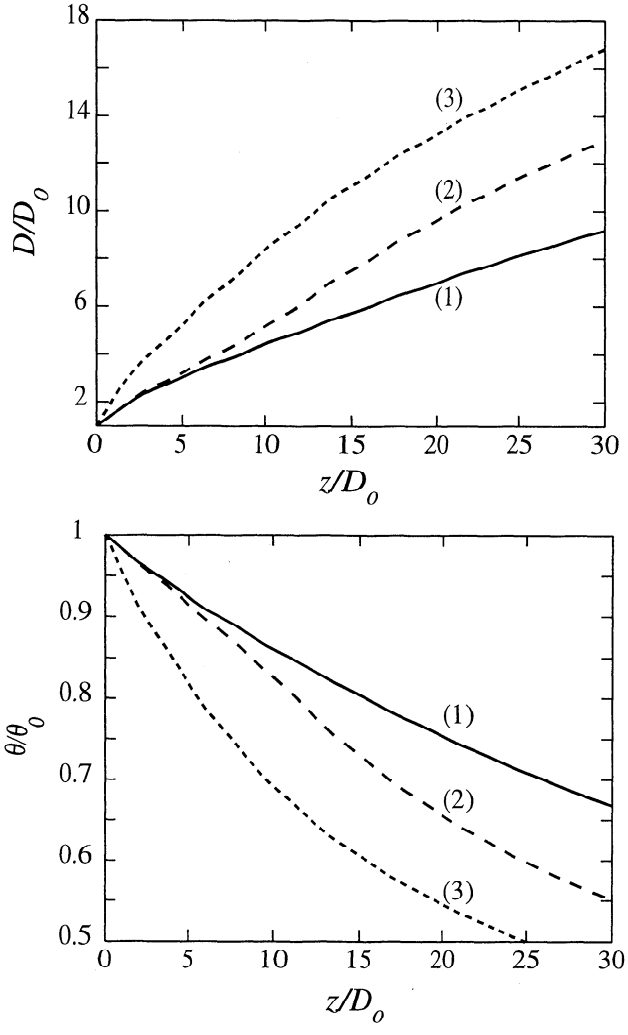

Figure 19. Bulk characteristics of the atmospheric eruption column for the parameters of Table 3 and for three different entrainment laws. (top) Radius of the eruption column as a function of height above the vent. Both variables are made dimensionless with the vent radius D_o. The three curves correspond to three different entrainment laws (equation (C7)) (1, $\lambda^* = 0.125$, $U_M = U$; 2, $\lambda^* = 0.125$, $U_M \neq U$; 3, $\lambda^* = 0.3, U_M \neq U$). The first entrainment law reproduces that of *Woods* [1988]. The third entrainment law leads to H=8xD_o, as observed in turbulent homogeneous jets [*Hinze*, 1975, p. 536]. (bottom). Average column temperature as a function of height for the same three entrainment assumptions. The entrainment law has a marked effect because it fixes the amount of mixing with cold atmospheric air.

marginal regions are described together but gives a reasonable temperature structure for our calculations. A more detailed approach would be beyond the scope of this paper.

We have considered three forms of the entrainment law and found significant differences in the predictions (Figure 19). All calculations discussed in the main text were made with the entrainment law of *Woods* [1988], i.e.,

$$U_e = 0.125\, U \left(\frac{\beta}{\alpha}\right)^{0.5}. \qquad \text{(C10)}$$

Above $z = H$, the centerline temperature starts decreasing more rapidly because of mixing with cold atmospheric air (Figure 12). There is a slight break in this evolution at $z = H$ due to the simple method used to parameterize entrainment. The calculation remains robust because all the conservation equations are satisfied, and, indeed, the average quantities have smooth evolutions.

Acknowledgments. This paper has benefited from two thorough anonymous reviews and from the detailed comments of Takehiro Koyaguchi. Funding was provided by the Programme National d'Étude des Risques Naturels, CNRS/INSU, France.

References

Alibidirov, M., and D. B. Dingwell, Magma fragmentation by rapid decompression, *Nature, 380*, 146–148, 1986.

Anilkumar, A.V., R. S. J. Sparks, and B. Sturtevant, Geological implications and applications of high-velocity two-phase flow experiments, *J. Volcanol. Geotherm. Res., 56*, 145–160, 1993.

Bagdassarov, N., and D. B. Dingwell, Frequency dependent rheology of vesicular rhyolite, *J. Geophys. Res., 98*, 6477–6487, 1993.

Bagdassarov, N., and D. B. Dingwell, Thermal properties of vesicular rhyolite, *J. Volcanol. Geotherm. Res., 60*, 179–191, 1994.

Baker, D. R., Granitic melt viscosities: Empirical and configurational entropy models for their calculation, *Am. Min., 81*, 126–134, 1996.

Bond, A., and R. S. J. Sparks, The Minoan eruption of Santorini, Greece, *J. Geol. Soc. London, 132*, 1–76, 1976.

Cashman, K. V., and M. T. Mangan, Physical aspects of magma degassing, II, Constraints on vesiculation processes from textural studies of eruptive products, *Rev. Mineral., 30*, 447–478, 1994.

Chung, J. N., and T. R. Troutt, Simulation of particle dispersion in an axisymmetric jet, *J. Fluid Mech., 186*, 199–222, 1988.

Clift, R., J. R. Grace, and M. E. Weber, *Bubbles, Drops, and Particles*, 380 pp., San Diego, Calif., 1978.

Dobran, F., Non-equilibrium flow in volcanic conduits and applications to the eruptions of Mt. St. Helens on May 18, 1980 and Vesuvius in AD79, *J. Volcanol. Geothermal Res., 49*, 285–311, 1992.

Dobran, F., A. Neri, and G. Macedonio, Numerical simulations of collapsing volcanic columns, *J. Geophys. Res., 98*, 4231–4259, 1993.

Eaton, J. K., and J. R. Fessler, Preferential concentration of particles by turbulence, *Int. J. Multiphase Flow, 20*, suppl., 169–209, 1994.

Erneux, T., and S. H. Davis, Nonlinear rupture of free films, *Phys. Fluids A, 5*, 1117-1122, 1993.

Gardner, J. E., H. Sigurdsson, and S. N. Carey, Eruption dynamics and magma withdrawal during the Plinian phase of the Bishop Tuff eruption, Long Valley caldera, *J. Geophys. Res., 96*, 8097 8111, 1991.

Gardner, J. E., R. M. E. Thomas, C. Jaupart, and S. Tait, Fragmentation of magma during plinian volcanic eruptions, *Bull. Volcanol., 58*, 144–162, 1996.

Giberti, G., C. Jaupart, and G. Sartoris, Steady-state operation of Stromboli volcano, Italy: Constraints on the feeding system, *Bull. Volcanol., 54*, 534-541, 1992.

Hardalupas, Y., A. M. K. P. Taylor, and J. H. Whitelaw, Velocity and particle-flux characteristics of turbulent particle-laden jet, *Proc. R. Soc. London, 1870*, 31–78, 1989.

Heiken, G., and F. McCoy Jr, Caldera development during the Minoan eruption, Thira, Cyclades, Greece, *J. Geophys. Res., 89*, 8441–8462, 1984.

Hinze, J.O., *Turbulence*, 790 pp., McGraw-Hill, New York, 1975.

Houghton, B. F., and C. J. N. Wilson, A vesicularity index for pyroclastic deposits, *Bull. Volcanol., 51*, 451–462, 1989.

Hurwitz, S. and O. Navon, Bubble nucleation in rhyolitic melts: Experiments at high pressure temperature and water content, *Earth Planet. Sci. Lett., 122*, 267–280, 1994.

Ishii, R., Y. Umeda, and M. Yuhi, Numerical analysis of gas-particle two phase flows, *J. Fluid Mech., 203*, 475–515, 1989.

Klug, C., and K. V. Cashman, Vesiculation of May 18, 1980, Mount St. Helens magma, *Geology, 22*, 468–472, 1994.

Li, X., H. Zhou, and C. Pozridikis, A numerical study of the shearing motion of emulsions and foams, *J. Fluid Mech., 286*, 379–404, 1995.

Macedonio, G., F. Dobran, and A. Neri, Erosion processes in volcanic conduits and an application to the AD79 eruption of Vesuvius, *Earth Planet. Sci. Lett., 121*, 267–280, 1994.

Mader H. M., Y. Zhang, J. C. Phillips, R. S. J. Sparks, B. Sturtevant, and E. Stolper, Experimental simulations of explosive degassing of magma, *Nature, 372*, 85–88, 1994.

Marble, F.E., Dynamics of dusty gases, *Annu. Rev. Fluid Mech., 2*, 397–446, 1970.

Neuville, D., P. Courtial, D. B. Dingwell, and P. Richet, Thermodynamic and rheological properties of rhyolite and andesite melts, *Contrib. Mineral. Petrol., 113*, 572–581, 1993.

Phillips J. C., S. J. Lane, A. M. Lejeune, and M. Hilton, Gum rosin-acetone system as an analogue to the degassing behavior of hydrated magmas, *Bull. Volcanol., 57*, 263–268, 1995.

Prevost, F., J. Boree, H. J. Nuglisch, and G. Charnay, Measurements of fluid/particle correlated motion in the far field of an axisymmetric jet, *Int. J. Multiphase Flow, 22*, 985–701, 1996.

Princen, H.M., Highly concentrated emulsions, I, Cylindrical systems, *J. Colloid Interface Sci., 75*, 246–270, 1979.

Proussevich, A. A., D. L. Sahagian, and A. T. Anderson, Dynamics of diffusive bubble growth in magmas: Isothermal case, *J. Geophys. Res., 98*, 22,283–22,308, 1993.

Prud'homme, R. K., and R. B. Bird, The dilatational properties of suspensions of gas bubbles in incompressible Newtonian and non-Newtonian fluids, *J. Non Newtonian Fluid Mech., 3*, 261–279, 1978.

Richet, P., Propriétés thermodynamiques des silicates fondus, 410 pp., Ph.D. thesis, Univ. Paris 7, 1992.

Shaw, H. R., Viscosities of magmatic liquids: An empirical method of predicition, *Am. J. Sci., 272*, 870–893, 1972.

Snyder D., E. Gier, and I. Carmichael, Experimental determination of the thermal conductivity of molten $CaMgSi_2O_6$

and the transport of heat through magmas, *J. Geophys. Res., 99*, 15,503–15,516, 1994.

Sparks, R. S. J., The dimension and dynamics of volcanic eruption columns, *Bull. Volcanol., 48*, 3–15, 1986.

Sparks, R. S. J., and L. Wilson, A model for the formation of ignimbrite by gravitational column collapse, *J. Geol. Soc. London, 132*, 141–151, 1976.

Sparks, R. S. J., and C. J. N. Wilson, The Minoan deposits: A review of their characteristics and interpretation, in *Thera and the Aegean World*, III, vol. 2, pp. 89–99, Thera Found., London, 1990.

Sparks, R. S. J., J. Barclay, C. Jaupart, H. M. Mader, and J. C. Phillips, Physical aspects of magmatic degassing, I, Experimental and theoretical constraints on vesiculation, *Volatiles in Magmas*, edited by M.R. Carroll and J. R. Holloway, *Rev. Mineral., 30* 413–445, 1994.

Stein, D. J., and F. J. Spera, Rheology and microstructure of magmatic emulsions theory and experiments, *J. Volcanol. Geotherm Res., 49*, 157–176, 1992.

Sugioka, I., and M. Bursik, Explosive fragmentation of erupting magma, *Nature, 373*, 689–692, 1995.

Taylor, G. I., The two coefficients of viscosity for an incompressible fluid containing air bubbles, *Proc. R. Soc. Lond. Ser. A, 226*, 34–39, 1954.

Thomas, N., C. Jaupart, and S. Vergniolle, On the vesicularity of pumice, *J. Geophys. Res., 99*, 15,633–15,644, 1994.

Turner, J. S., *Buoyancy Effects in Fluids*, 398 pp., Cambridge Univ. Press, New York, 1973.

Valentine, G., and K. Wohletz, Numerical models of Plinian eruption columns, *J. Geophys. Res., 94*, 1867–1887, 1989.

Vrij, A., Possible mechanism for the spontaneous rupture of thin, free liquid films, *Disc. Faraday Soc., 42*, 23–30, 1966.

Wilson, L., Explosive volcanic eruptions, III, Plinian eruption columns, *Geophys. J. R. Astron. Soc., 45*, 543–556, 1976.

Wilson, L., R. S. J. Sparks, and G. P. L. Walker, Explosive volcanic eruptions, IV, The control of magma properties and conduit geometry on eruption column behavior, *Geophys. J. R. Astron. Soc., 63*, 117–148, 1980.

Wilson, C. J. N., and B. J. Houghton, Eruptive mechanisms in the Minoan eruption: Evidence for pumice vesicularity, in *Thera and the Aegean World*, III, vol. 2, pp 105–113, Thera Found., London, 1990.

Woods, A. W., The fluid dynamics and thermodynamics of eruption column, *Bull. Volcanol., 50*, 169–193, 1988.

Woods, A. W., The dynamics of explosive volcanic eruptions, *Rev. Geophys., 33*, 495–530, 1995.

Woods, A. W., and C. P. Caulfield, A laboratory study of explosive volcanic eruptions, *J. Geophys. Res., 97*, 6699–6712, 1992.

C. Jaupart, Institut de Physique du Globe, 4. Pl. Jussieu, F-75252, Paris cedex 5, France. (e-mail: cj@ccr.jussieu.fr)

E. Kaminski, Institut de Physique du Globe, 4. Pl. Jussieu, F-75252, Paris cedex 5, France. (e-mail: kaminski@ipgp.jussieu.fr)

(Received May 28, 1996; revised February 10, 1997; accepted February 19, 1997.)